2005 IEEE/RSJ International Conference on Intelligent Robots and Systems

Steering Characteristics of an Exploration Rover on Loose Soil based on All-Wheel Dynamics Model

Genya Ishigami
Dept. of Aerospace Engineering
Tohoku University
Aoba 6-6-01, Sendai, 980-8579, Japan
ishigami@astro.mech.tohoku.ac.jp

Kazuya Yoshida
Dept. of Aerospace Engineering
Tohoku University
Aoba 6-6-01, Sendai, 980-8579, Japan
yoshida@astro.mech.tohoku.ac.jp

***Abstract*— In this paper, steering characteristics of an exploration rover on loose soil is studied. Analysis of the steering characteristics is a key to plan and control the motion trajectory of a rover. Traditionally, such analysis has been made based on a model called "bicycle model." In that model, a four-wheel car-like vehicle is approximated by a two-wheel bicycle-like vehicle with the fore-wheels and the rear-wheels paired. However, the bicycle model does not show a good performance when a vehicle travels off-road. In order to analyze the steering characteristics of a vehicle on loose soil, the authors develop a model that respects the dynamics of each wheel's slip and skid behavior. The developed model is called All-Wheel Dynamics Model. In the all-wheel dynamics model, the behavior of each wheel on loose soil is modeled based on terramechanics. The motion trajectory of the vehicle is obtained by numerical simulation using the wheel-and-vehicle dynamics model. The validity of the proposed model is examined by the experiments of a wheel and a vehicle using simulated lunar-surface soil. The experimental results show that the proposed model provides a better approximation than the traditional bicycle model.**

***Index Terms*— Exploration rover, Steering characteristics, Terramechanics**

I. Introduction

The use of mobile robots (rovers) in a planetary mission significantly expands the exploration areas, then increases the scientific return of the mission. Today, planetary rovers are expected to travel a longer distance and perform more complex tasks in order to accomplish more challenging mission goals than ever. In the last decade, a considerable amount of research has been done in various aspect for the development of planetary rovers [1]-[13].

The terrain of a major planetary body such as Mars or Moon is mostly covered with loose soil called *regolith*. The rover is required to travel on such highly challenging terrain, climbing a hill, traversing a slope, and negotiating with craters, boulders, rocks or stones spread over the terrain. On loose soil, the wheels of the rover easily slip and loose their traction. On the other hand, on rocky surface, the rover might become unstable or, in the worst case, tips over. Hence, it is necessary to investigate the static and dynamic behavior of the rover, taking into account the interaction between the wheels and the soil. The research field of the soil mechanics is called *terramechanics*. In this field, the analysis of a wheel-soil traction mechanism and the modeling of the stress distribution underneath the wheel have been studied [5]-[7]. Iagnemma et al. successfully applied those terramechanic models to the issues of planetary robotics, and developed an on-line method to identify soil parameters (cohesion stress and friction angle) using onboard sensory data [8][9]. Grand et al. developed a novel simulation model which considers the flow of loose soil under the wheel [10]. The present authors also investigated the wheel-soil interaction for the modeling and control of a rover taking a terramechanics-based approach [11]-[13].

The issue addressed in this paper is the steering characteristics of a rover on loose soil. A traditional approach to analyze the steering characteristics of an on-road vehicle uses an approximated model called the "bicycle model." However, the bicycle model would not show good approximation when a vehicle travels off-road. Particularly when a vehicle dynamically skids on loose soil, the difference becomes greater. Therefore, the main focus of this paper is the development of a better steering model of a vehicle that respects each wheel's slip and skid behavior on loose soil. We call the model "All-Wheel Dynamics Model," since it takes the motion dynamics of all wheels into account.

A key issue of this paper is the development of a wheel-soil contact model for steering maneuver. The basic study of the contact model for rigid wheels on loose soil has been developed in the terramechanics field, as pointed above. However, the investigation of the lateral (side) forces of the wheel on loose soil has been left as an open issue. The modeling of the side force is absolutely necessary in order to discuss the steering characteristics. The present authors, therefore, have been investigating a model for the sides forces that gives good approximation [13].

In general, the side forces are produced by the shear stress of the soil under the wheel [7]. However, on loose soil, the wheels have certain amount of sinkage and then another force called "bulldozing resistance" is generated on the side face of the wheel. Paying close attention to the wheel-sink phenomenon, the wheel contact model is formulated. Dynamic behavior of a wheel is characterized by two parameters; one is slip ratio and the other is slip angle. The proposed model uses these parameters as a state variable, then both the longitudinal and lateral forces are formulated as a function of the slip ratio and the slip angle.

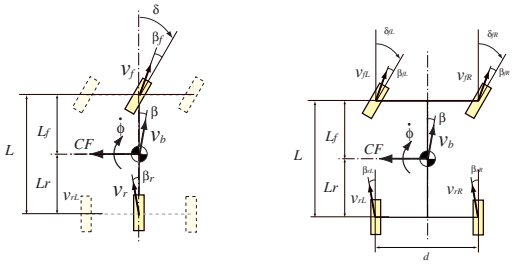

(a) : Bicycle mdoel (b) : All-wheel dynamics model

Fig. 1. Bicycle model and all-wheel dynamics model

The validity of the wheel contact model is verified using a single wheel experimental test bed. In this test bed, forces produced by a single wheel are measured when it travels at an arbitrarily given velocity, rotates at a given angular velocity, with a given steering angle. Through the experiments, the propriety of the contact model is confirmed. The validated contact model is then plugged into the all-wheel dynamics model.

The motion trajectories of a rover obtained from two different models, the bicycle model and the all-wheel dynamics model, are compared with the corresponding experimental trajectory. In this way, the advantage of the all-wheel dynamics model over the bicycle model is clarified.

This paper is organized as follows. The following section (Section II) introduces the bicycle model as a traditional approach and the all-wheel dynamics model is suggested as an improved one. In Section III, the wheel contact model is referred. Particularly, the modeling of the side force is focused. Experimental results are presented in Section IV along with the discussion on the validity of the wheel contact model. In Section V, the proposed all-wheel dynamics model is elaborated. Steering motion trajectories of a vehicle on loose soil are obtained using the proposed model, then compared with the experimental results obtained from the corresponding rover test bed,

II. Vehicle Model for Steering Characteristics

To discuss the steering characteristics, a bicycle model has been traditionally employed. The bicycle model, shown in Fig.1-(a), approximates that the fore left and right wheels have the same behavior, whereas the rear left and right wheels might have a different behavior compared to the front pair but equivalent to each other [14].

In the bicycle model, an instantaneous turning radius ρ of a vehicle is derived as:

$$\rho = L/\{\delta(1 + K_s v_b^2)\} \tag{1}$$

where v_b is a vehicle's traveling velocity, L is a wheel base, and δ is a steering angle. Additionally, stability-factor K_s is defined as:

$$K_s = -m \cdot (L_f/C_r - L_r/C_f)/(2L^2) \tag{2}$$

where m is a mass of the vehicle, L_f (L_r) is a wheel base of a fore (rear) wheel. C_f (C_r) is a cornering stiffness of the fore (rear) wheel, which is derived from a cornering force with respect to a slip angle.

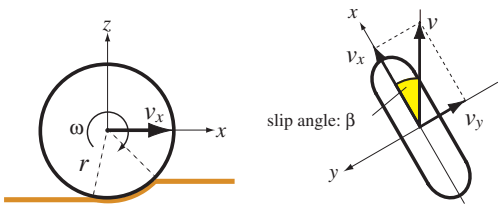

Fig. 2. Wheel coordinate system

According to our steering experiments on loose soil which is described later, the bicycle model does not show a good performance in the steering trajectory, because each wheel acts dissimilar behaviors respectively on off-road. That is also easily deduced from our general experiences.

Therefore, as shown in Fig.1-(b), we develop an all-wheel dynamics model in order to deal with the each wheel's traveling behavior. The all-wheel dynamics approach needs explicit model for the interaction between each wheel and soil. Then, the section III refers to the wheel contact model so as to treat the traveling behavior of the each wheel.

III. Wheel Contact Model Based on Terramechanics

The following analysis deals with a rigid wheel rotating on loose soil. A wheel coordinate system is defined using a right-hand frame as shown in Fig.2, where the longitudinal direction is denoted by x, the lateral direction by y, and the vertical direction by z. The coordinate frame turns according to the steering action of the wheel (the yaw rotation around z axis) but does not rotate with the driving motion of the wheel (the pitch rotation around y axis).

A. Slip ratio and slip angle

When a wheel is traveling on a loose soil, the wheel can slip both in the longitudinal and lateral directions. The slip in the longitudinal direction is measured by "slip ratio," which is defined as a function of the longitudinal traveling velocity v_x and the circumference velocity of the wheel $r\omega$:

$$s = \begin{cases} (r\omega - v_x)/r\omega & (r\omega > v_x : \text{driving}) \\ (r\omega - v_x)/v_x & (r\omega < v_x : \text{braking}) \end{cases} \tag{3}$$

The slip ratio takes a value between -1 and 1.

On the other hand, the slip in the lateral direction is measured by "slip angle," which is defined by the longitudinal and lateral traveling velocities v_x, v_y of the wheel as follows:

$$\beta = \tan^{-1}(v_y/v_x) \tag{4}$$

B. Normal stress and shear stress

Based on terramechanics models, the stresses under the wheel can be modeled as shown in Fig.3-(a). The normal stress $\sigma(\theta)$ is described according to [11]-[13]:

$$\sigma(\theta) = \sigma_m \cdot \left(\frac{\cos\theta - \cos\theta_f}{\cos\theta_m - \cos\theta_f} \right)^n \tag{5}$$

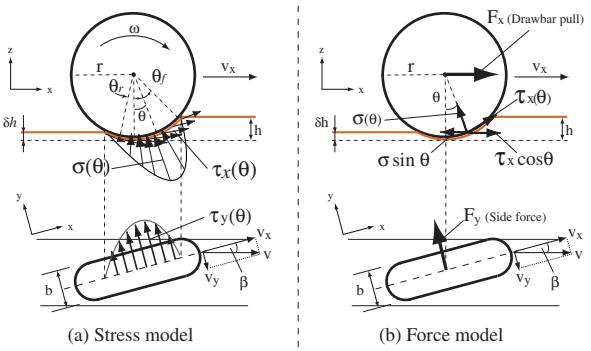

(a) Stress model (b) Force model

Fig. 3. Wheel contact model on loose soil

$$\sigma(\theta) = \sigma_m \cdot \left(\frac{\cos\{\theta_f - \frac{\theta-\theta_r}{\theta_m-\theta_r}(\theta_f-\theta_m)\} - \cos\theta_f}{\cos\theta_m - \cos\theta_f} \right)^n \quad (6)$$

$$(\theta_m \le \theta \le \theta_f)$$

$$(\theta_r \le \theta \le \theta_m)$$

The maximum stress σ_m is defined by the following equation [7]:

$$\sigma_m = r^n(k_c/b + k_\phi)(\cos\theta_m - \cos\theta_f)^n \quad (7)$$

where, k_c, k_ϕ and n are the soil-specific parameters. b is the width of the wheel.

The shear stresses $\tau_x(\theta)$ and $\tau_y(\theta)$ are written by the same expressions:

$$\tau_i(\theta) = (c + \sigma(\theta)\tan\phi)[1 - e^{-j_i(\theta)/k_i}] \quad (i = x, y) \quad (8)$$

The symbols used in the equation (8) are listed as follows:

c : cohesion stress of the soil
ϕ : internal friction angle of the soil
k_i : shear displacement in each direction

Also, j_x and j_y are soil deformations in each direction, which are formulated as a function of the wheel angle θ:

$$j_x(\theta) = r[\theta_f - \theta - (1-s)(\sin\theta_f - \sin\theta)] \quad (9)$$

$$j_y(\theta) = r(1-s)(\theta_f - \theta)\cdot\tan\beta \quad (10)$$

C. Traction force F_x

A general force model for a rigid wheel on loose soil is presented in Fig.3-(b).

Using the normal stress $\sigma(\theta)$ and the shear stress in x direction $\tau_x(\theta)$, a traction force F_x that exerts from the soil to the wheel is calculated by the integral from the entry angle θ_f to the exit angle θ_r [5]-[7]:

$$F_x = rb\int_{\theta_r}^{\theta_f} \{\tau_x(\theta)\cos\theta - \sigma(\theta)\sin\theta\} d\theta \quad (11)$$

D. Side force F_y

The present authors have modeled the side force F_y as follows [13]:

$$F_y = F_u + F_s \quad (12)$$

As shown in Fig.3 and Fig.4, F_u is a force produced by the shear stress in y direction underneath the wheel. F_s is a reaction force generated by a bulldozing phenomenon on a side face of the wheel.

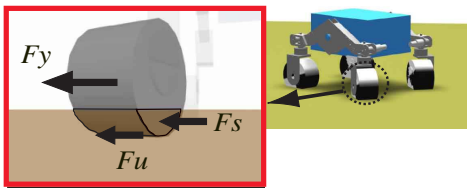

Fig. 4. Lateral (side) forces acting on the wheel

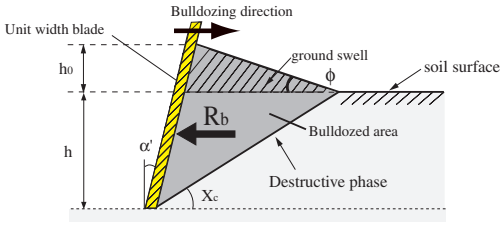

Fig. 5. Estimation model of bulldozing resistance

Then, equation (12) can be rewritten as:

$$\begin{aligned} F_y &= F_u + F_s \\ &= \int_{\theta_r}^{\theta_f} \{rb\cdot\tau_y(\theta)\}\, d\theta \\ &\quad + \int_{\theta_r}^{\theta_f} \{R_b\cdot(r - h(\theta)\cos\theta)\}\, d\theta \end{aligned} \quad (13)$$

In order to derive the force F_s, we applied Hegedus's bulldozing resistance estimation. As descried in Fig.5, a bulldozing resistance R_b is generated to a blade with an unit width when it moves towards the soil. According to the Hegedus's theory, the bulldozing area is defined by a destructive phase which is modeled by a planar surface and the ground swell which is generated on the soil surface. In the case of a horizontally placed wheel, an angle of approach α should be zero. Then, R_b can be calculated as a function of a wheel sinkage h:

$$R_b(h) = D_1(h\cdot c + h^2\cdot D_2\cdot\rho) \quad (14)$$

$$D_1(X_c,\phi) = \cot X_c + \tan(X_c + \phi) \quad (15)$$

$$D_2(X_c,\phi) = (\cot X_c + \cot^2 X_c/\cot\phi)/2 \quad (16)$$

In the above equations, ρ means a soil density. The wheel sinkage h is given as a function of wheel angle θ [11]-[13]:

$$h(\theta) = r(\cos\theta - \cos\theta_f) \quad (17)$$

Also, based on Bekker's theory [6], the destructive angle X_c can be approximated as described below:

$$X_c = 45^\circ - \phi/2 \quad (18)$$

E. Numerical simulation of contact forces

Using the above equations, the numerical simulations were carried out to evaluate the wheel's contact forces as a function of the slip ratio and the slip angle.

TABLE I

SIMULATION PARAMETERS AND VALUES

parameter	value	unit
c	0.80	[kPa]
ϕ	37.2	[deg]
r	0.09	[m]
b	0.11	[m]
k_x	$0.014 \sim 0.023$	[m]
k_y	$0.016 \sim 0.022$	[m]
k_c	1.37×10^3	$[\mathrm{N/m^{n+1}}]$
k_ϕ	8.14×10^5	$[\mathrm{N/m^{n+2}}]$
n	1.0	

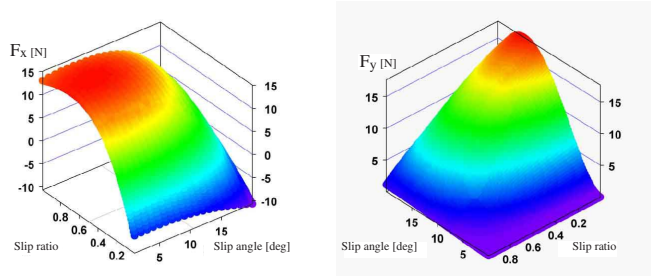

(a) : Traction force F_x (b) : Side force F_y

Fig. 6. Numerical simulation results on contact forces

Simulation condition

Simulations were performed under the same condition as the following experiments. For both the simulations and the experiments, a rigid wheel with a diameter of 0.18 [m] and a width of 0.11 [m] was used. We also used "Lunar Regolith Simulant" as an experimental soil. This is a simulated lunar surface soil in terms of similar material components and mechanical characteristics.

The parameters used in the simulations are listed in Table I. The values of those parameters were identified from other experiments [12].

Simulation result

Fig.6 depicts an example of simulation results. These figures respectively describe the traction force F_x and the side force F_y according to various slip ratios s and slip angles β.

From these figures, it is seen that the traction force is saturated approximately around $s = 0.6$ and has a maximum value at $s = 1.0$, whereas the side force has a maximum value at $s = 0$. It is also interesting to know that the side force decreases constantly and finally becomes almost zero at $s = 1.0$. Note that the result of zero-side force at $s = 1.0$ is quite reasonable from general experiences; when traction wheels start spinning on snowy or icy road, the vehicle loses its steering control.

In addition, the traction force decreases depending on the slip angle but not remarkably. On the other hand, the larger the slip angle is the larger the lateral force becomes.

IV. SINGLE WHEEL EXPERIMENT

In order to verify the validity of the wheel contact model, experiments are carried out using a test bed for a single wheel locomotion [13].

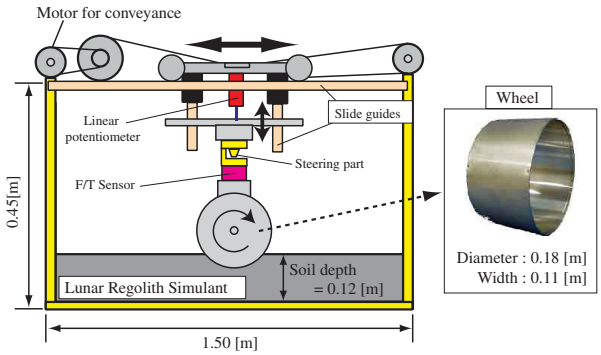

Fig. 7. Schematic view of the single wheel test bed

A. Experimental conditioin

Fig.7 shows the schematic view of the single wheel test bed. The test bed is constituted by a conveyance unit and a wheel driving units. A steering angle (which is equivalent to the slip angle in this case) can be set between the conveyance unit and the wheel. The conveyance and the wheel rotating velocities are individually measured by encoders that are mounted at the each corresponding driving motor. The forces generated by the wheel locomotion are measure by a 6-axis force/torque sensor located between the steering part and the wheel.

In the following experiments, the wheel is set to rotate with a constant circumference velocity ($r\omega$=0.036 [m/s]) by a driving motor mounted inside of the wheel. The conveyance velocity is controlled so that the slip ratio is set from 0 to 0.9 with a step of 0.1. The slip ratio can be constant during every single run. The slip angle is also set constant during every experiment of the single run. The value of the slip angle is given from 0 to 16 degrees with a step of 4 degrees. The load on the wheel is 64.7 [N].

B. Experimental results

The experimental measurements of the traction and the side forces are respectively plotted in Fig.8 and Fig.9, for each slip angle from 4 to 16 degrees. Corresponding theoretical curves calculated by the wheel contact model are also drawn in the figures.

These graphs confirm such characteristics as the side force decreases along with the slip ratio and increases according to the slip angle. The differences between the measured forces and the theoretical values are relatively small. These results validate that the proposed wheel contact model represents the wheel's traveling behaviors and the contact forces with a reasonable precision.

V. DYNAMICS SIMULATION BASED ON ALL-WHEEL DYNAMICS MODEL

Dynamics simulations based on the all-wheel dynamics model are conducted in order to analyze the rover's steering characteristics. Furthermore, rover's motion trajectories that are respectively obtained from 1) a steering experiment using a rover test bed, 2) the bicycle model, and 3) the all-wheel dynamics model are compared.

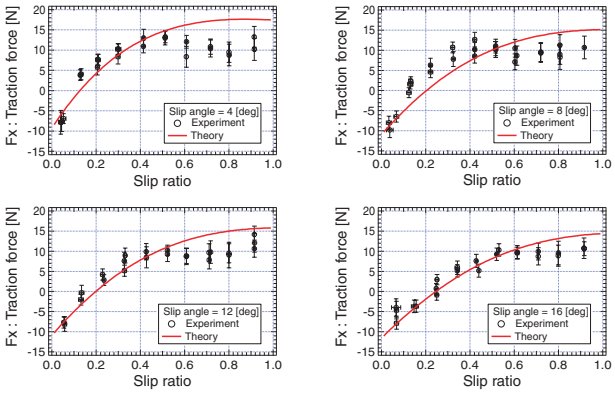

Fig. 8. Experimental results (slip ratio - traction force)

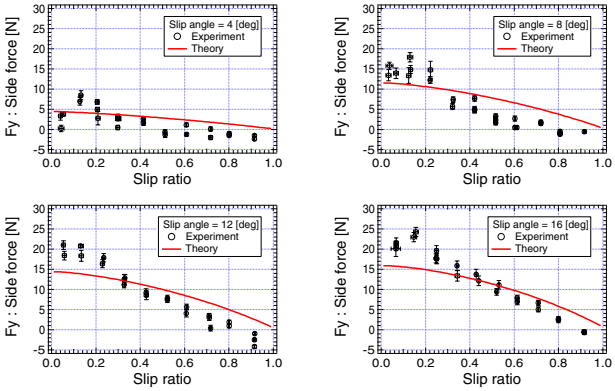

Fig. 9. Experimental results (slip ratio - side force)

A. All-wheel dynamics model of a vehicle

The all-wheel dynamics model consists of two models; one is the wheel contact model which was discussed in Section III, and the other is a dynamics model of the vehicle.

The dynamic motion equation of the vehicle is generally written as:

$$\mathbf{H}\begin{bmatrix}\dot{\mathbf{v}}_0\\ \dot{\omega}_0\\ \ddot{\mathbf{q}}\end{bmatrix}+\mathbf{C}=\begin{bmatrix}\mathbf{F}_0\\ \mathbf{N}_0\\ \tau\end{bmatrix}+\mathbf{J}^T\begin{bmatrix}\mathbf{F}_e\\ \mathbf{N}_e\end{bmatrix} \tag{19}$$

where the symbols used in the above equation are listed as:

- $\mathbf{H}$: inertia matrix of the vehicle
- $\mathbf{C}$: velocity depending term
- $\mathbf{v}_0$: translational velocity of the body
- ω_0 : angular velocity of the body
- $\mathbf{q}$: angle of each joint of the vehicle
- $\mathbf{F}_0$: forces acting to the center of gravity of the body
- $\mathbf{N}_0$: torques acting to the center of gravity of the body
- τ : torques acting to each joint of the vehicle
- $\mathbf{J}$: Jacobian matrix
- $\mathbf{F}_e = \left[f_{w1}^T, \cdots, f_{wn}^T\right]^T$: external forces acting to the center of gravity of the each wheel
- $\mathbf{N}_e$: torques acting to the center of gravity of the each wheel

Note that, the external forces to the each wheel $f_{wi}(i = 1, \cdots, n)$ is given by the wheel contact model such as equations (11) and (12).

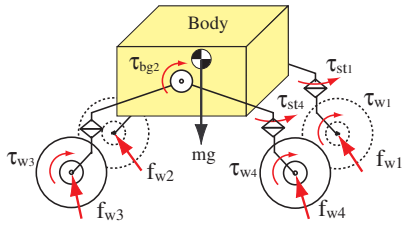

Fig. 10. Dynamics model of the rover

The above equations are general and can be applied to a vehicle with any configuration. In the following discussion, we will compare the numerical results with the experimental results using our rover test bed with four-wheel independent drive and steer. A schematic model of the rover test bed is shown in Fig.10. Specific parameters for the rover kinematics and dynamics are identified from the test bed and used in the simulation.

The motion trajectory of the rover with a given traveling and steering conditions is numerically obtained by solving the equation equation (19) successively.

B. Simulation procedure

The simulation procedures using the all-wheel dynamics model are summarized as follows:

1) Input steering angles δ_{wi} and angular velocities ω_{wi} to the each wheel $(i = 1, \cdots, 4)$.
2) Calculate external forces f_{wi} acting to the each wheel using the wheel contact model.
3) Determine $\mathbf{F}_0$, $\mathbf{N}_0$, $\mathbf{F}_e$, $\mathbf{N}_e$ and τ.
4) Slove equation (19), then obtain the rover's position, orientation and velocity.
5) Calculate slip ratios and slip angles of the each wheel, then return to 2).

The simulation was performed by using an in-house software, named *SpaceDyn*. The *SpaceDyn* is the form of MATLAB toolbox for the numerical computations of kinematics and dynamics of the articulated body systems with a moving base [15][16]. We used it to obtain the forward dynamics solution of equation (19).

C. Steering experiment using rover test bed

In the steering experiments, the rover test bed travels with a given angular velocity and a steering angle. The rover test bed weighs 35 [kg]. Each wheel is controlled to travel with a constant wheel angular velocity and a constant steering angle by an on-board computer. We measured a motion trajectory of the rover using a 3D optical sensor. Force/torque sensors are also mounted on upper part of the each wheel to measure the forces generated by the corresponding wheel. The test field is evenly covered with the Lunar Regolith Simulant. Overviews of the steering experiment is shown in Fig.11-(a).

D. Discussion of the all-wheel dynamics model

Fig.11-(b) shows a computer graphics model to represent the result of the dynamics simulation using the all-wheel dynamics model. An experimental result of the rover's trajectory

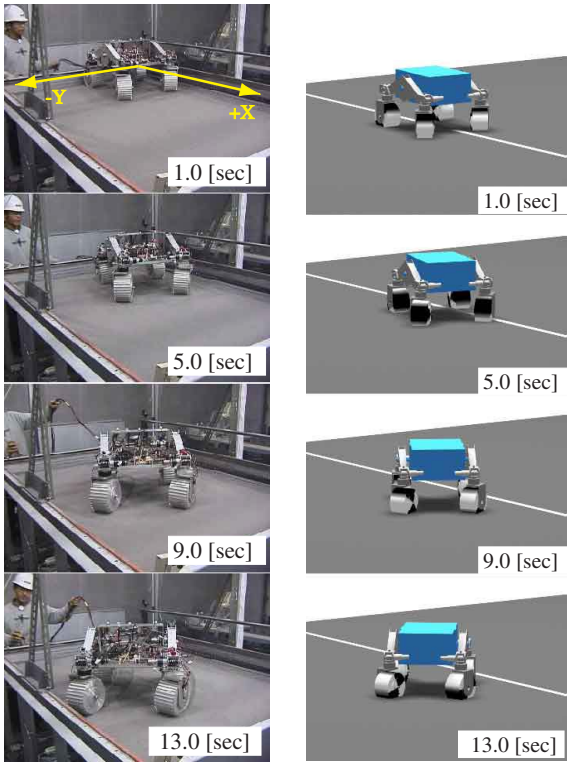

(a) : experiment (b) : all-wheel dynamics model

Fig. 11. Comparison of the rover's steering motion

is shown in Fig.12. The average traveling velocity of the rover was 0.1 [m/s]. The trajectories obtained from the bicycle model and the all-wheel dynamics model are also drawn in the same figure, respectively.

From Fig.12, the trajectory derived from the all-wheel dynamics model well reproduces the experimental result with a reasonable precision (within 0.05 [m] error).

On the other hand, the bicycle model-based trajectory has relatively large difference from the experiment. The reason is that the bicycle model is based on the approximation of zero slip ratios (no slip) and small slip angles. However on loose soil, the wheels slip and skid dynamically. In fact, the wheels had about 0.45 in slip ratios and $3 \sim 6$ [deg] in slip angles in this experiment. The all-wheel dynamics model can calculate the slip ratios and the slip angles within allowable errors.

Note that, the bicycle model may offer a good approximation when the rover travels on-road with a relatively fast traveling velocity. The all-wheel dynamics model, however, can simulate the dynamic behavior even if the rover travels off-road with any given traveling velocity.

VI. Conclusion

In this paper, the steering characteristics of an exploration rover were investigated. The wheel contact model was developed based on terramechanics. The model was validated with the numerical simulation and the experiments of a single wheel.

The steering motion of a rover was dynamically simulated using the all-wheel dynamics model. The result of the steering

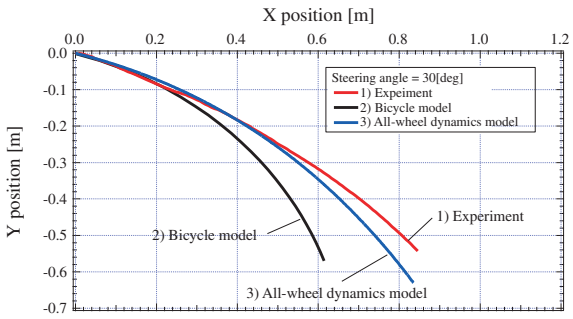

Fig. 12. Trajectory comparison of the experiment and the simulation

trajectory represents that the proposed model provides a better approximation to the experimental result than the traditional bicycle model.

The bicycle model may be useful for 4-wheel conventional car-like on-road vehicles though, the all-wheel dynamics model is able to deal with any vehicles with arbitrary number of wheels and chassis configurations, as long as the dynamics model of the vehicle is developed correctly.

The all-wheel dynamics model will be useful for future practical issues, such as planning a motion trajectory and controlling the steering motion to follow the given trajectory.

References

[1] http://marsrovers.jpl.nasa.gov/home/index.html (as of May 2005)
[2] I. Nakatani, K. Matsumoto, T. Izumi; "SELENE-B: Proposed Lunar Mission with Lander and Rover," Proc. of the 7th Int. Symp. on Artificial Intelligence, Robotics and Automation in Space, 2003.
[3] R. Volpe and S. Peters; "Rover Technology Development and Infusion for the 2009 Mars Science Laboratory Mission," Proc. of the 7th Int. Symp. on Artificial Intelligence, Robotics and Automation in Space, 2003.
[4] K. Rajan, et. al.; "MAPGEN: Mixed Initiative Planning and Scheduling for the Mars '03 MER Mission," Proc. of the 7th Int. Symp. on Artificial Intelligence, Robotics and Automation in Space, 2003.
[5] M. G. Bekker; "Introduction to Terrain-Vehicle Systems," The University of Michigan Press, 1969.
[6] M. G. Bekker; "OFF-THE-ROAD LOCOMOTION," The University of Michigan Press, 1960.
[7] J. Y. Wong; "Theory of Ground Vehicles," John Wiley & Sons, 1978.
[8] K. Iagnemma, H. Shibly, S. Dubowsky; "On-Line Traction Parameter Estimation for Planetary Rovers," Proc. of the 2002 IEEE Int. Conf. on Robotics and Automation, pp. 3142–3147, 2002.
[9] K. Iagnemma and S. Dubowsky,; "Mobile Robot in Rough Terrain," Springer Tracts in Advanced Robotics, vol.12, 2004.
[10] C. Grand, F. Ben Amar, P. Bidaud; "A Simulation System for Behaviour Evaluation of Off-road Mobile Robots," 4th Int. Conf. on Climbing and Walking Robots, 2001.
[11] K. Yoshida, T. Watanabe, N. Mizuno, G. Ishigami, "Terramechanics-Based Analysis and Traction Control of a Lunar/Planetary Rover," 4th Int. Conf. on Field and Service Robotics, 2003.
[12] K. Yoshida, N. Mizuno, G. Ishigami, A. Miwa, "Terramechanics-Based Analysis for Slope Climbing Capability of a Lunar/Planetary Rover," 24th Int. Symp. on Space Technology and Science, 2004.
[13] K. Yoshida, G. Ishigami; "Steering Characteristics of a Rigid wheel for Explaration on Loose Soil," Proc of the 2004 IEEE Int. Conf. on Intelligent Robots and Systems, pp. 3995–4000, 2004.
[14] Z. Shiller and S. Sunder; "EMERGENCY MANEUVERS OF AUTONOMOUS VEHICLES," Proc of Int. Federation of Automatic Control, pp. 393-398, 1996.
[15] K. Yoshida ; "The SpaceDyn: a MATLAB Toolbox for Space and Mobile Robots," J. of Robotics and Mechatronics, vol.12 no.4, pp. 411-416, 2000.
[16] http://www.astro.mech.tohoku.ac.jp/spacedyn